Commun. Comput. Phys.
doi: 10.4208/cicp.OA-2022-0197

Vol. **35**, No. 1, pp. 139-159
January 2024

Variational Low-Light Image Enhancement Based on Fractional-Order Differential

Qianting Ma[1], Yang Wang[2] and Tieyong Zeng[3,*]

[1] *School of Mathematics and Statistics, Nanjing University of Information Science and Technology, Nanjing, Jiangsu Province 210044, China.*
[2] *Department of Mathematics, The Hong Kong University of Science and Technology, Hong Kong SAR, China.*
[3] *Department of Mathematics, The Chinese University of Hong Kong, Hong Kong SAR, China.*

Received 17 July 2022; Accepted (in revised version) 14 November 2022

Abstract. Images captured under insufficient light conditions often suffer from noticeable degradation of visibility, brightness and contrast. Existing methods pose limitations on enhancing low-visibility images, especially for diverse low-light conditions. In this paper, we first propose a new variational model for estimating the illumination map based on fractional-order differential. Once the illumination map is obtained, we directly inject the well-constructed illumination map into a general image restoration model, whose regularization terms can be viewed as an adaptive mapping. Since the regularization term in the restoration part can be arbitrary, one can model the regularization term by using different off-the-shelf denoisers and do not need to explicitly design various priors on the reflectance component. Because of flexibility of the model, the desired enhanced results can be solved efficiently by techniques like the plug-and-play inspired algorithm. Numerical experiments based on three public datasets demonstrate that our proposed method outperforms other competing methods, including deep learning approaches, under three commonly used metrics in terms of visual quality and image quality assessment.

AMS subject classifications: 52B10, 65D18, 68U05, 68U07
Key words: Low-light image, image enhancement, fractional-order, variational methods.

1 Introduction

Image enhancement refers to the process of highlighting certain information of an observed low-visibility image, as well as weakening or removing any unnecessary information according to specific needs [1]. With the prevalence of webcams and camera phones,

*Corresponding author. *Email addresses:* qtma@nuist.edu.cn (Q. Ma), yangwang@ust.hk (Y. Wang), zeng@math.cuhk.edu.hk (T. Zeng)

the problem of image enhancement has become extremely challenging as images captured by digital devices may influenced by various conditions such as insufficient light, bad weather, unknown noise and so on. The enhanced image quality directly affects high-level image analysis and understanding, which is widely used in many scientific, engineering and medical applications. Thus, developing advanced image enhancement techniques are of great significance and urgency.

Retinex theory is first introduced to model the perception of human vision and is used to remove illumination effects [2]. According to the basic assumption of the Retinex theory [3, 4], an observed image can be decomposed into the illumination and reflectance components. Due to the ill-posedness of the decomposition problem, numerous approaches [5–7] have been proposed to mitigate the degradation caused by low-light conditions. These methods of low-light enhancement are mainly divided into three categories. Roughly speaking, the first one is two-step methods, which estimate the illumination map and then make use of image restoration methods to recover the desired light-enhanced scene. For example, LIME [8] first estimate the illumination map by using a structure prior and the enhancement can be achieved by using gamma transformation. The second method is the joint filtering method [9]. This kind of method aims to transfer the important structural details of the guidance to the target image in the filtering process. The third method is to estimate illumination map and reflectance component simultaneously by solving a joint minimization problem with image priors on both them. The image priors include sparsity regularization [10], fractional-order regularization [11], high-order total variation regularization [12, 13] and low rank prior [14].

Variational interpretations of Retinex are the set of enhancement algorithms [15, 16]. The first variational framework was proposed by Kimmel et al. [17] to estimate the illumination, and its objective function is established based on the smooth illumination assumption. In [8], the illumination map was first constructed by finding the maximum intensity of each pixel in all channels (i.e. bright channel). Then, the initial illumination map is refined by adding the L_1 norm on the first order derivative of the illumination. Afterwards, bright channel prior has been used in other works [18, 19] to eliminate the black halo and suppress color distortion. However, it always encounters the problems of dispersion of light in light dominant areas, over enhancement in bright regions and unwanted artifacts. Li et al. [20] used L_1 norm to constrain the piece-wise smoothness of the illumination, and adopted a fidelity term between the gradient of the reflectance and an adjusted version of the gradient of the input image, so that the structural information of the reflectance can be strengthened. Gu et al. [21] performed the fractional-order gradient total variation regularization on both the reflectance and illumination components to control the regularization extent more flexibly. Park et al. [22] proposed a L_2 norm minimization based a variational Retinex model by using a spatially adaptive weight map, which is generated by combining the local variance map and bright channel prior [23]. Gu et al. [24] performed L_2 norm on the gradient of the illumination and L_1 norm on the reflectance in the image domain along with a fidelity term to estimate the illumination and the reflectance simultaneously. Ren et al. [25] proposed a reasonable camera

response model to adjust each pixel to the desired exposure according to the estimated exposure ratio map. Wang et al. [26] proposed a lightness-order-error measure for the naturalness preservation to assess enhanced images. They argued that the relative order of illumination in different areas should not be changed drastically. Fu et al. [27] proposed an illumination estimating algorithm based on morphological closing to decompose a low-light image into a reflectance image and an illumination image. They argued that the enhanced result can be obtained by fusing the derived inputs with corresponding weights in a multi-scale fashion. However, different kinds of priors may not model the real reflectance and the piecewise smoothness of the illumination. This may impose a limitation in restoring low-light images.

Deep convolutional neural networks (CNNs) have been successful in achieving impressive results on numerous low-level computer vision tasks [28–30]. Various CNNs-based algorithms have been proposed to improve the subjective and objective quality of low-light images [31,32]. For example, Liu et al. [33] first established optimization models based on the Retinex rule to formulate the latent structures of the illumination map, and then unrolled the iteration process with deep priors to obtain the holistic structure of the enhancement network. LightNet [34] worked as an enhancer to refine the illumination map of the low-light image. EnlightenGAN [35] used Generative Adversarial Networks that regarded the low-light enhancement as a domain transfer learning task by finding the mapping between low-light and normal-light domains. ZeroDCE [36] formulated light enhancement as a task of image-specific curve estimation with deep networks. Deep lightening network [37] regarded the low-light enhancement as a residual learning problem that is to estimate the residual between low-light and normal-light images. He et al. [38] combined traditional methods and CNNs to achieve image brightness enhancement, color recovery and denoising. LLRNet [39] performed joint contrast enhancement and denoising of input by exploiting the learning of subband coefficients instead of learning original images. Xu et al. [40] presented a neural network that leverages an attention to context encoding module to adaptively select low-frequency information for recovering the low-frequency layer and noise removal in the first stage and select high-frequency information for detail enhancement in the second stage.

The aforementioned methods show impressive results on enhancing low-light images. In practice, sensor-specific noise universally appears in low-light images and heavily relies on paired training data for its removal. Also, uneven illumination, incorrect focus, low contrast and high noise are prevalent in low-illumination images. In the presence of such adverse conditions, the performance of almost existing enhancing methods noticeably decreases. Additionally, the parameters of learning-based methods are fixed after training and can not generalize well to the changeable real-world scenarios. Thus, how to develop efficient image enhancement algorithms that are robust to both image noise and various types of illumination has drawn attention in recent years. Most of these robust image enhancement approaches assume that the desired high-quality image can be reliably identified by designing different kinds of priors. In practice, the real reflectance can not be reliably identified, e.g. unknown noise. Also, in many sit-

uations, the illumination map can be estimated by training on few public datasets. This is mainly because it is extremely challenging to simultaneously take a low-light image and a normal-light image of the same visual scene. Hence, it limits the practical values of learning-based methods.

In this paper, we separate the task of low-light image enhancement into two stages. The first stage is to estimate a smooth illumination map that can facilitate the enhancement, and the second stage is to extract a normal-light image from an observed low-light image. To find a well-constructed illumination map, instead of considering the integer-order total variation of latent image, we propose a novel illumination estimation model with two regularization terms based on fractional-order differential. One regularization term is designed to constrain spatial smoothness on the refined illumination by the L^1-regularized term. The other regularization term serves the purpose of measuring the similarity between the fractional derivative of the refined illumination and the fractional derivative of the input image by L^2-regularized term. Once the illumination map is found, then in the second stage, the enhancement is obtained by directly injecting the refined illumination component into a general image restoration model. Instead of designing specific priors on the reflectance, we model the regularization term as adaptive mappings. Since the regularization term can be arbitrary, we directly apply some excellent off-the-shelf denoising methods, hence, our proposed method requires no training at all, making the solving procedure efficient and flexible. This adaptive regularizer is shown to have significantly better noise-removal property and restoration performance than other competing methods. The proposed model is numerically solved based on the plug-and-play inspired algorithm to accomplish an efficient implementation.

The remainder sections of this paper are organized as follows. In Section 2, our proposed method is described in detail. In Section 3, the effective discretization and numerical scheme are presented. Some numerical experiments are presented and evaluated in Section 4. Finally, the conclusion is presented in Section 5.

2 Proposed

In Retinex theory [41], an observed image S can be decomposed into two element-wise multiplied factors which are the reflectance component R and the illumination map I. The formula can be expressed by

$$S = R \cdot I, \tag{2.1}$$

where the operator $\cdot$ means element-wise multiplication. We need to estimate both the illumination map I and the reflectance component R. Most existing models for low-light image regularization contains different image priors only on the restored image. This may be insufficient when considering image formation models. The fractional-order total variation regularization has been widely used in image restoration because of its ability in nonlinearly maintaining the low frequency features and simultaneously enhance details in the area that the intensity does not change obviously [42–44]. We will adopt

the fractional-order total regularization in the illumination estimation for low-light image enhancement. Besides, expect for the fidelity term of the data, we hope that the fractional-order derivative of a refined illumination is consistent with that of the original degraded image. To enrich the variety of image formation models, we propose an illumination estimation method which exploits two regularization terms based on fractional differential. Our model is shown as follows,

$$\min_I \|I^0-I\|_2^2+\lambda\|\nabla^\alpha S_m-\nabla^\alpha I\|_2^2+\mu\|G\circ\nabla^\beta I\|_1, \tag{2.2}$$

where I^0 can be viewed as an initial illumination, λ and μ are positive parameters, ∇^α and ∇^β represent two fractional-order derivatives, $\|\cdot\|_2$ and $\|\cdot\|_1$ designate the L_2 norm and L_1 norm, respectively. The weights in matrix G are calculated as $G_x=1/\nabla_x I^0$, $G_y=1/\nabla_y I^0$, where ∇_x and ∇_y denote first-order derivative along horizontal and vertical dimension, respectively. Researchers [45] try to initialize a illumination map by using the maximum intensity of all channels, say R, G, B, at a certain location from input images , i.e.

$$\hat{I}(x)=\max_{c\in\{R,G,B\}} S^c(x), \tag{2.3}$$

where S^c denotes the corresponding channel of the input S. However, the initialization in (2.3) may have a drawback when applied to a low-light image with uneven illumination conditions. They often over-enhance the input image, especially on relatively bright areas. Instead of using the initial illumination in (2.3), we initialize the illumination by

$$I^0=(\hat{I})^\tau, \tag{2.4}$$

where $\tau\in(0,1)$, $\hat{I}$ can be simply expressed by (2.3). It is worth noting the properties of the function in (2.4): small intensity values in dark areas will be large, and large intensity values in relatively bright areas will be restrained. Additionally, $\nabla^\alpha S_m(x)$ is defined by

$$\nabla^\alpha S_m(x)=\max_{c\in\{R,G,B\}} \nabla^\alpha S^c(x). \tag{2.5}$$

The role of each term in objective (2.2) is interpreted below,

- $\|I^0-I\|_2^2$ narrows the error between the initial illumination and a refined one.
- $\|\nabla^\alpha S_m-\nabla^\alpha I\|_2^2$ measures the similarity between the fractional derivative of the refined illumination and the fractional derivative of input images.
- $\|G\circ\nabla^\beta I\|_1$ constrains spatial smoothness on the refined illumination.

Once I is obtained, we enter into the second stage of our method, where we use a general image restoration model to enhance a low-light image with noise-removal. However, we do not explicitly fix the regularization term in the second stage. Instead, we replace the steps related to the regularization term by some adaptable mapping. We leave the implementation to Section 3.

3 Numerical implementation

3.1 Discrete forms of fractional-order operators

Since the Grünwald-Letnikov (G-L) fractional order derivative [46] can be viewed as an extension of the discrete form of the finite difference scheme for the integer-order derivatives, we will introduce the G-L definition of the fractional-order derivative ∇_x^α and ∇_y^β. For a real function $I:\Omega\to\mathbb{R}$, where $\Omega\subseteq\mathbb{R}^2$ is a bounded open set, the fractional-order derivative is represented as

$$\nabla^\alpha I=(\nabla_x^\alpha I,\nabla_y^\alpha I),\quad \alpha\in\mathbb{R}^+. \tag{3.1}$$

The G-L discrete form of the fractional-order derivatives ∇_x^α and ∇_y^α is defined as follows,

$$\nabla_x^\alpha I(x,y)=\sum_{l=0}^{L-1}(-1)^l C_\alpha^l I(x-l,y),\quad \nabla_y^\alpha I(x,y)=\sum_{l=0}^{L-1}(-1)^l C_\alpha^l I(x,y-l), \tag{3.2}$$

where C_α^l is the generalized binomial coefficient, that is,

$$C_\alpha^l=\frac{\Gamma(\alpha+1)}{\Gamma(l+1)\Gamma(\alpha-l+1)} \tag{3.3}$$

and $\Gamma(\cdot)$ is the gamma function. It is noticing that the fractional-order differential is related with more pixels than the integer-order one by selecting the parameter L larger than 3 in the G-L fractional-order derivatives (3.2), the fractional-order derivative is more favorable to structure preservation in image restoration. In our experiment, we fix the parameter L in (3.2) equals to 15. Let $(\nabla_x^\alpha)^T$ and $(\nabla_y^\alpha)^T$ be the adjoint operators of ∇_x^α and ∇_y^α, then they are defined as

$$(\nabla_x^\alpha)^T I(x,y)=\sum_{l=0}^{L-1}(-1)^l C_\alpha^l I(x+l,y),\quad (\nabla_y^\alpha)^T I(x,y)=\sum_{l=0}^{L-1}(-1)^l C_\alpha^l I(x,y+l). \tag{3.4}$$

3.2 The first stage

Many optimization methods can be applied to solve the minimization problem [47–50]. In this subsection, we employ the alternative direction minimization algorithm [51] for solving the model (2.2). Let us replace the terms $\nabla^\alpha I$ and $\nabla^\beta I$ with auxiliary variables K and P, respectively. Then the objective function in (2.2) can be rewritten as follows,

$$\min_{I,K,P}\|I^0-I\|_2^2+\lambda\|\nabla^\alpha S_m-K\|_2^2+\mu\|G\circ P\|_1,\quad s.t.\quad \nabla^\alpha I=K,\quad \nabla^\beta I=P. \tag{3.5}$$

To employ the alternative direction minimization algorithm, we introduce two new Lagrangian multipliers L_1 and L_2 and reformulate the minimization problem (3.5) as

$$\min_{I,K,P}\|I^0-I\|_2^2+\lambda\|\nabla^\alpha S_m-K\|_2^2+\mu\|G\circ P\|_1+\phi_1(L_1,\nabla^\alpha I-K)+\phi_2(L_2,\nabla^\beta I-P), \tag{3.6}$$

and ϕ_1, ϕ_2 can be defined by

$$\phi_1(L_1,\nabla^\alpha I-K)=\frac{\omega_1}{2}\|\nabla^\alpha I-K\|_2^2+\langle L_1,\nabla^\alpha I-K\rangle,$$
$$\phi_2(L_2,\nabla^\beta I-P)=\frac{\omega_2}{2}\|\nabla^\beta I-P\|_2^2+\langle L_2,\nabla^\beta I-P\rangle,$$

where $\langle\cdot,\cdot\rangle$ represents matrix inner product, ω_1, ω_2 are positive penalty scalar, and L_1, L_2 are Lagrangian multipliers. Our model can be solved through the following iterations.

Computation of I: Dropping the terms unrelated to I, the problem of finding I from (3.6) is reduced to minimize the following subproblems,

$$\arg\min_I \|I^0-I\|_2^2+\phi_1(L_1,\nabla^\alpha I-K)+\phi_2(L_2,\nabla^\beta I-P),$$

which can be solved efficiently by the Fast Fourier Transform (FFT) as follows,

$$I^{i+1}=\mathcal{F}^{-1}\Big(\frac{\mathcal{F}(2\hat{I})+\sum_d\overline{\mathcal{F}\big((\nabla_d^\alpha)^T(\omega_1^iK^i-L_1^i)\big)}+\sum_d\overline{\mathcal{F}\big((\nabla_d^\beta)^T(\omega_2^iP^i-L_2^i)\big)}}{2+\omega_1^i\sum_d\overline{\mathcal{F}(\nabla_d^\alpha)}\mathcal{F}(\nabla_d^\alpha)+\omega_2^i\sum_{d\in\{x,y\}}\overline{\mathcal{F}(\nabla_d^\beta)}\mathcal{F}(\nabla_d^\beta)}\Big),\tag{3.7}$$

where $\mathcal{F}(\cdot)$ and $\mathcal{F}^{-1}(\cdot)$ denote the FFT operator and the inverse FFT operator, respectively. $\overline{\mathcal{F}(\cdot)}$ stands for the complex conjugate of $\mathcal{F}(\cdot)$. ∇_d^α with the parameter $d\in\{x,y\}$ denotes the horizontal (vertical) fractional-order differential operators.

Computation of K: By collecting the K involved terms from (3.6), we minimize the energy (3.6) with respect to the variable K as follows,

$$\arg\min_K \lambda\|\nabla^\alpha S_m-K\|_2^2+\phi_1(L_1,\nabla^\alpha I-K).\tag{3.8}$$

It's easy to show that the energy (3.6) is minimized by K with

$$K^{i+1}=\frac{2\lambda\nabla^\alpha S_m+\omega_1^i\nabla^\alpha I^{i+1}+L_1^i}{2\lambda+\omega_1^i}.\tag{3.9}$$

Computation of P: For solving the sub-problem with respect to the variable P, we minimize the energy (3.6) as follows,

$$\arg\min_p \mu\|G\circ P\|_1+\phi_2(L_2,\nabla^\beta I-P).\tag{3.10}$$

The sub-problem (3.10) can be solved explicitly using a generalized shrinkage formula [52] as follows,

$$P^{i+1}=S_{\mu G/\omega_2^i}\Big[\nabla^\beta I^{i+1}+L_2^i/\omega_2^i\Big],\tag{3.11}$$

where $S_\phi[x]=sign(x)\max(|x|-\phi,0)$, and all operations are element-wise.

Computation of L_1, L_2, ω_1, ω_2: The Lagrangian multiplier matrixes L_1 and L_2, penalty terms ω_1 and ω_2 can be updated as follows,

$$\begin{aligned}
&L_1^{i+1}=L_1^i+\omega_1^i(\nabla^\alpha I^{i+1}-K^{i+1}),\\
&L_2^{i+1}=L_2^i+\omega_2^i(\nabla^\beta I^{i+1}-P^{i+1}),\\
&\omega_1^{i+1}=\omega_1^i\delta_1,\quad \omega_2^{i+1}=\omega_2^i\delta_2,\\
&\delta_1>0,\quad \delta_2>0.
\end{aligned} \tag{3.12}$$

To sum up, the numerical implementation for the illumination estimation part can be summarized as below.

1st stage (illumination map estimation)

Input: low-light image S, fraction-order α and β, regularization parameters λ and μ, and parameters ω_1, ω_2, δ_1, δ_2, and ϵ.
Initialization: $I^0\in\mathbb{R}^{m\times n}$, $L_1^0=L_2^0=\mathbf{0}\in\mathbb{R}^{2m\times n}$, $\omega_1^0>0$, $\omega_2^0>0$,
Do i = 0,1,$\cdots$, until $\|I^{i+1}-I^i\|_2^2/\|I^{i+1}\|_2^2<\epsilon$.
1. Compute I^{i+1} by (3.7).
2. Compute K^{i+1} by (3.9).
3. Compute P^{i+1} by (3.11).
4. Update L_1^{i+1}, L_2^{i+1}, ω_1^{i+1}, and ω_2^{i+1} by (3.12).
Output: the refined illumination map I.

3.3 The second stage

As mentioned before, our enhancement result is obtained by directly injecting the solution I of (2.2) into the following restoration model with an adaptable mapping,

$$\min_R\{\|S-R\cdot I\|_2^2+\phi(R)\}. \tag{3.13}$$

Introducing the auxiliary variable Q, problem (3.13) can be reformulated as below by using the half-quadratic splitting method [53],

$$\min_{R,Q}\{\|S-R\cdot I\|_2^2+\nu\|R-Q\|_2^2+\phi(Q)\}, \tag{3.14}$$

where ν is a positive parameter. The problem (3.14) is solved by an alternating scheme,

$$R^i=\arg\min_R\{\|S-R\cdot I\|_2^2+\nu\|R-Q^{i-1}\|_2^2\}, \tag{3.15}$$

$$Q^i=\arg\min_Q\{\nu\|R^i-Q\|_2^2+\phi(Q)\}. \tag{3.16}$$

The sub-problem (3.15) can be solved analytically as follows,

$$R^i=\frac{S\cdot I+\nu Q^{i-1}}{I\cdot I+\nu 1}, \tag{3.17}$$

where 1 denotes the matrix with all ones. Since the regularization term in (3.13) can be arbitrary, we directly apply some excellent off-the-shelf denoising methods, making the solving procedure efficient and flexible. In this paper, we choose a non-supervised method BM3D [54] and a recursive filter (RF) [55] with a pre-trained denoising model to conduct our ablation study of the selection of denoisers. For BM3D, the denoiser can be downloaded from (http://www.cs.tut.fi/ foi/GCF-BM3D/). For RF, the denoiser can be downloaded from (http://inf.ufrgs.br/eslgastal/DomainTransform/). Hence, (3.16) can be solved as follows,

$$Q^i = \text{Denoiser}(R^i, \nu). \tag{3.18}$$

Since different denoising methods can be applied directly, our method requires no training at all. To sum up, the numerical implementation for the restoration part can be summarized as below.

2nd stage (enhanced result restoration)
Input: illumination map I, low-light image S and ν.
1. Initialize: $R^0 = S$.
2. Do i = 0,1,$\cdots$, until $\|R^i - R^{i-1}\|_2^2 / \|R^i\|_2^2 < \epsilon$.
(b) Compute Q^i by solving (3.18).
(b) Compute R^i by solving (3.17).
Output: enhanced result R.

4 Numerical experiments

4.1 Experiment settings

To evaluate the effectiveness of our method, we compare our method with other competing methods, including LIME [8], NPE [26], MF [27], SR [20], LNet [34], RUAS [33], EnGAN [35], LCR [25], and DCE [36], on images from various scenes. We make an objective evaluation of images on three public datasets, including NPE dataset [26], LOL dataset [7] and GladNet dataset [56], where the LOL dataset contains sensible noises to hinder the enhancement. We also adopt Peak Signal-to-Noise Ratio (PSNR) [57] and Structure Similarity (SSIM) [58] which are widely used in image restoration field to measure the quality of the estimation. As for PSNR, it is most commonly used to measure the quality of image reconstruction, a higher PSNR generally indicates that the reconstruction is of higher quality. As for SSIM, it can be used as a evaluation metric that gives further consideration for structure similarity. The value of SSIM ranges from 0 to 1, and larger values of SSIM can represent better similarity. In addition, we also use a blind quality assessment, i.e. autoregressive-based image sharpness metric (ARISM). ARISM performs well in accordance with object assessment on the inevitable effect of color information on visual perception to sharpness, lower ARISM values represent that image contrasts have been better improved.

The experimental program is developed of MATLAB (R2019a, 64-bit, maci64). All results are tested on a MacBook Pro platform, macOS with Intel core i7, 2.2GHz, 16GB, 2400 MHz. We set $\nu=0.2$ for all datasets. If not specifically stated, empirical parameters ω_1^0, ω_2^0, δ_1, and δ_2 are set at 0.0001, 0.001, 0.1, 0.3, respectively, and ϵ in the stopping criterion is 10^{-3}.

4.2 Ablation study

Hyper-parameter Settings: α and β are fractional orders controlling the regularization of the estimated illumination map. To illustrate the influence of our model with respect to α and β, we measure how the PSNR values are influenced by fractional-order α and β. For this purpose, we fix $\lambda=0.001$ and $\mu=0.5$, and vary the parameters α and β from 0.5 to 2.9 for a low-light image shown in Fig. 6 collected from the LOL dataset [7]. By observation in Fig. 1, we can see that PSNR values tend to increase when $\alpha,\beta\geq 0.5$. Please note that higher PSNR values represent better visual quality. The PSNR is one of the basic image restoration metrics to validate the proposed algorithm. As shown in Fig. 1, we can see that our proposed method achieves higher PSNR scores when $\alpha,\beta\geq 2$. Specifically, results with $2\leq\alpha,\beta\leq 2.5$ have higher PSNR values. This argues that regularization terms based on fractional differential can achieve more promising enhanced results than regularization terms based on integer differential. Hence, we use $(\alpha,\beta)=(2.1,2.3)$ as our default setting.

The parameter τ in (2.4) is used as a controller for restraining intensity values in relatively bright areas. To evaluate the impact of our initialization scheme with different τ, we test how the convergence rate is affected by using our initialization scheme with different choice of τ. For this purpose, we show the convergence curves of the error of $\|R^{n+1}-R^n\|_2^2/\|R^n\|_2^2$ for different selection of τ. The results show that the convergence curves can rapidly drop to 10^{-3} and change slightly as the number of iterations increases. It argues that our method converges rapidly in only a few steps. Moreover, from the

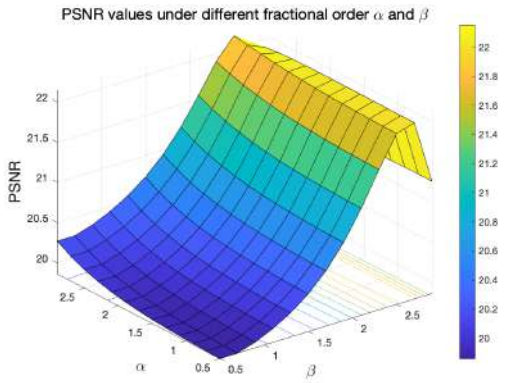

Figure 1: Ablation study of fractional-order α and β settings.

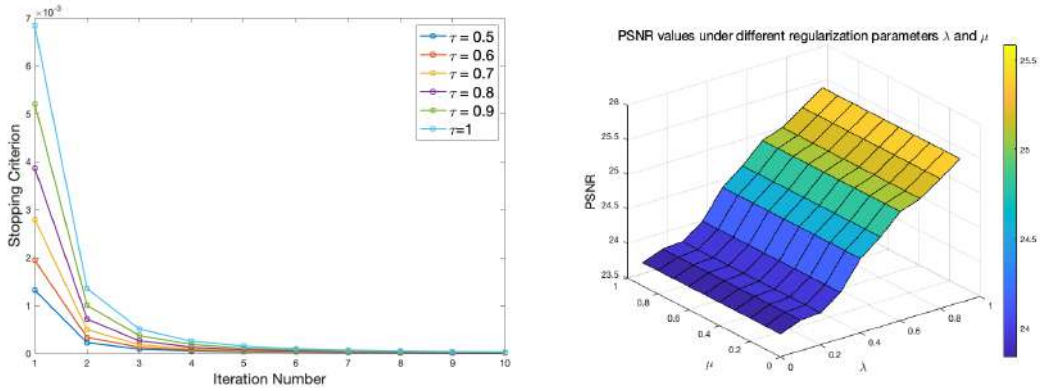

Figure 2: From left to right: ablation studies of our initialization scheme with different τ and regularization parameters λ and μ settings, respectively.

curves shown in Fig. 2, we can see that the convergence rate has been already less than 10^{-3} in the first two iterations when $\tau<1$. It argues that our initialization scheme with $\tau<1$ can accelerate the convergence of our algorithm. However, when $\tau=1$, more iterations are required to achieve the stop tolerance. For simplicity, we fix the exponent τ of power functions in (2.4) to be 0.5.

Regularization-parameter settings: λ and μ are positive parameters balancing two regularization terms. In order to test the influence of regularization terms in our model, we select a low-light image from the LOL dataset [7] shown in Fig. 6 and discuss the PSNR values obtained by using different λ and μ. As shown in Fig. 2, we can find that the PSNR values tend to ascend when fixing μ and varying the λ from 0 to 1. It argues that the fidelity term between the fractional-order gradient of a estimated illumination and the fractional derivative of input images can somehow assist our model to obtain better effects on enhancing a low-light image. However, when fixing λ, PSNR values seem to change slightly as μ increases. It argues that our method is insensitive to the change of μ. Additionally, as shown in Fig. 2, PSNR values can be higher with carefully selection of λ, $\mu>0$. It argues that two regularization terms based on the fractional-order gradient of a refined illumination can somehow improve the performance of our model on lighting up low-illumination images.

Runtime comparisons: As our method is applicable to incorporate existing off-the-shellf denoising methods, as illustrated in Section 3.3, we select a non-supervised method BM3D [54] and a recursive filter (RF) [55] with a pre-trained denoising model to conduct our ablation study of selection denoisers. For the 20 low-light images collected from the LOL dataset [7], the average computational time for our method with two different denoisers are listed as follows: our method with RF denoiser 0.2252s, our method with BM3D denoiser 10.6750s. As analyzed, the runtime depends highly on the selection of denoisers. With better denoisers, our method may achieve better results. In other words,

the most time-consuming part of our method is restoring a enhanced image by MATLAB. A faster version can hugely reduce the computational time, which is left as future work.

4.3 Comparisons with state-of-the-arts

Fig. 3 presents several visual comparisons against the aforementioned methods on the GladNet dataset [56]. Fig. 3(i) is our result with $\lambda = 0.01$ and $\mu = 5$ by using the RF denoiser. According to Fig. 3, we zoom in on some details in the bounding boxes. The recovered image produced by LIME [8] contains noises that is especially noticeable in the zoomed area. The results of MF [27] and NPE [26] remain dark to some extent. LNet [34]

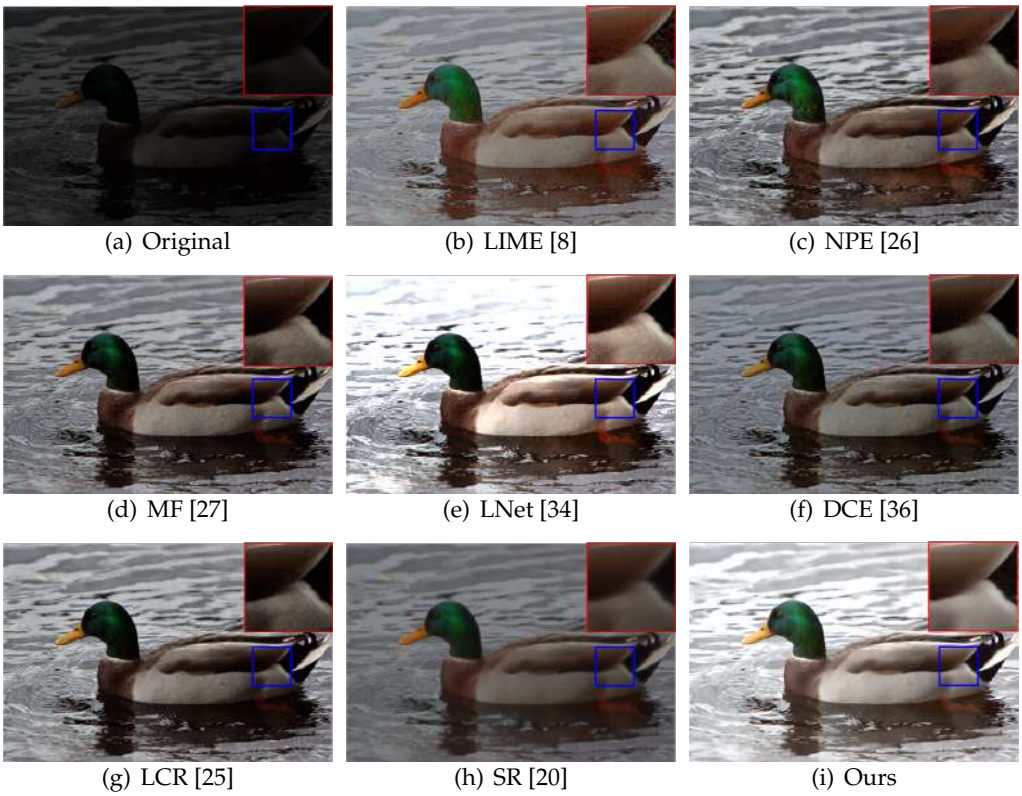

(a) Original (b) LIME [8] (c) NPE [26]

(d) MF [27] (e) LNet [34] (f) DCE [36]

(g) LCR [25] (h) SR [20] (i) Ours

Figure 3: Comparisons with state-of-the-art low-light image enhancement methods on the GladNet dataset [56].

Table 1: Quantitative analysis for Fig. 3.

	SR [20]	LIME [8]	NPE [26]	MF [27]	LNet [34]	DCE [36]	LCR [25]	**Ours**
PSNR	10.9247	14.9045	14.1484	13.8239	17.2457	12.6109	15.4196	**21.4322**
SSIM	0.5804	0.7789	0.7957	0.7811	0.7960	0.8339	0.7908	**0.8812**
ARISM	2.8250	3.3185	3.4559	3.2040	3.5813	3.3304	3.1981	**2.7010**

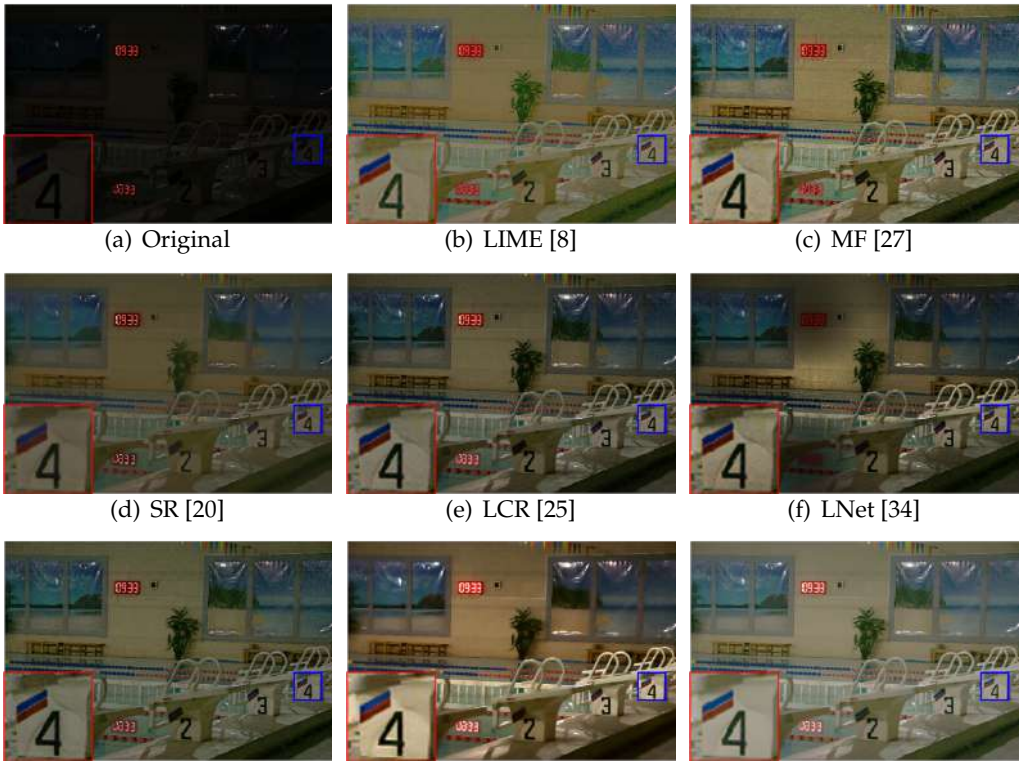

(a) Original (b) LIME [8] (c) MF [27]

(d) SR [20] (e) LCR [25] (f) LNet [34]

(g) DCE [36] (h) RUAS [33] (i) Ours

Figure 4: Comparisons with state-of-the-art low-light image enhancement methods on the LOL dataset [7].

Table 2: Quantitative analysis for Fig. 4.

	SR [20]	LIME [8]	RUAS [33]	MF [27]	LNet [34]	DCE [36]	LCR [25]	**Ours**
PSNR	17.8192	23.7874	20.7995	22.8143	16.0270	20.0621	18.2096	**24.1971**
SSIM	0.8052	0.8860	0.6698	0.8972	0.7488	0.9090	0.8998	**0.9147**
ARISM	3.3581	3.6487	3.6432	3.7787	3.7511	3.8952	3.8250	**3.3254**

can not give a significant enhancement result. DCE [36], LCR [25] and SR [20] can light up low-light images slightly. In contrast, our proposed method can successfully enhance the image content while suppressing noise. As shown in Table 1, our method can achieve higher PSNR and SSIM values and lower ARISM values than that of other competing methods. It indicates that our method can successfully enhance the overall quality of images and generate images that are visually more pleasant.

Fig. 4 shows a low-light image with varying illumination and results of various enhancement algorithms. Fig. 4(i) is our result with $\lambda = 0.1$ and $\mu = 5$ by using the BM3D denoiser. From the comparison, one can notice that LNet [34] provides limited visibility improvement in the shaded areas. The image enhanced by SR [20] still has compara-

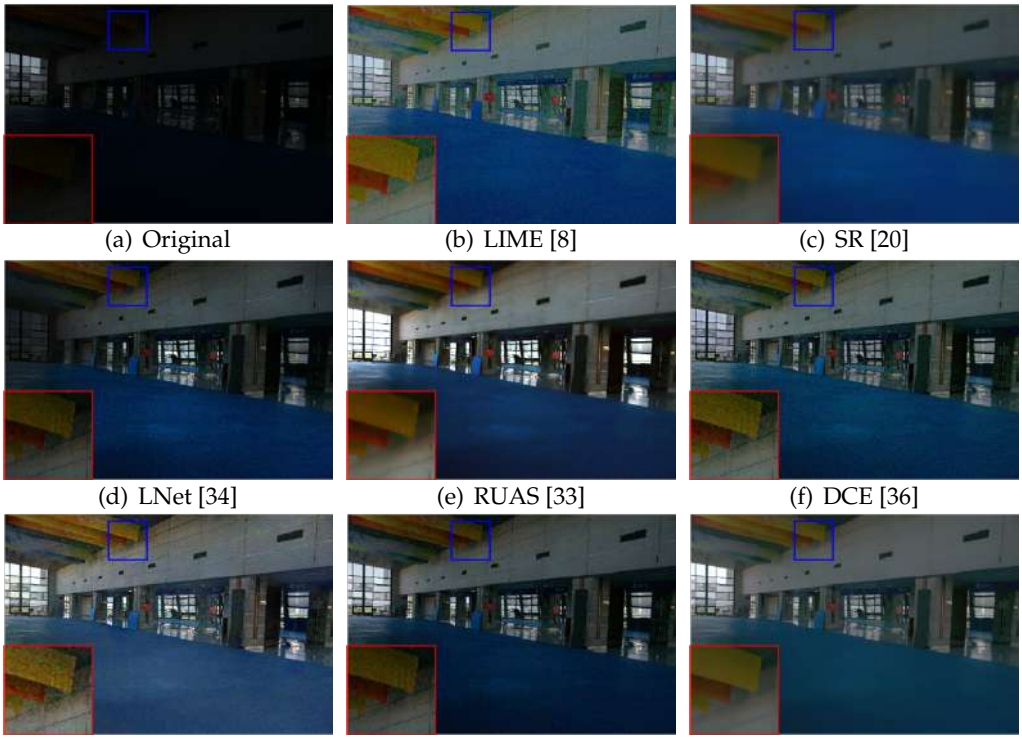

(a) Original (b) LIME [8] (c) SR [20]

(d) LNet [34] (e) RUAS [33] (f) DCE [36]

(g) EnGAN [35] (h) LCR [25] (i) Ours

Figure 5: Comparisons with state-of-the-art low-light image enhancement methods on the LOL dataset [7].

Table 3: Quantitative analysis for Fig. 5.

	LIME [8]	RUAS [33]	SR [20]	LNet [34]	DCE [36]	EnGAN [35]	LCR [25]	**Ours**
PSNR	22.1084	21.7586	22.1946	16.0049	22.7732	22.3606	20.9650	**28.0280**
SSIM	0.7536	0.7178	0.9106	0.7133	0.7638	0.8127	0.7136	**0.9247**
ARISM	3.7719	3.8406	3.2415	4.1449	4.2189	3.1337	4.1728	**2.9397**

tively low visibility. DCE [36] and LCR [25] give improved visibility but amplify noises in dark regions. The results of LIME [8], MF [27] and RUAS [33] give much improved visibility. However, they fail to suppress noise in the enhanced images. Overall, when processing noisy images, all these algorithms are sensitive to noise more or less. In terms of PSNR, SSIM and ARISM, our method is the best. It again indicates that our method can successfully enhance image contents while suppressing noises.

Fig. 5 shows a challenge case in the luminosity enhancement. We can hardly see anything in the bounding box. Fig. 5(i) is our result with $\lambda = 0.01$ and $\mu = 1$ by using the BM3D denoiser. As can be observed in visual comparisons, all results generated by different methods can enhance the visibility of low-light images to some extent. From the comparison, we can clearly see that LNet [34] and LCR [25] can brighten the dark

(a) Original (b) SR [20] (c) MF [27]

(d) LIME [8] (e) LCR [25] (f) LNet [34]

(g) DCE [36] (h) EnGAN [35] (i) Ours

Figure 6: Comparisons with state-of-the-art low-light image enhancement methods on the LOL dataset [7].

Table 4: Quantitative analysis for Fig. 6.

	SR [20]	MF [27]	LIME [8]	LCR [25]	LNet [34]	DCE [36]	EnGAN [35]	**Ours**
PSNR	20.4168	23.6441	22.4414	22.9476	14.5470	24.9617	20.6196	**24.9643**
SSIM	0.7472	0.7452	0.8447	0.8335	0.6454	0.7735	0.7747	**0.8876**
ARISM	2.8441	3.8166	3.5368	3.7769	3.7327	3.8326	2.9925	**2.7359**

regions slightly. LIME [8] can sufficiently enhance the input image but it also generate noises in dark regions. RUAS [33] fails to well process the very dark areas. DCE [36] and EnGAN [35] can reveal the image content in low-visibility regions but they can not suppress the noise in low-illumination regions. In Table 3, we also report the PSNR, SSIM and ARISM values of enhanced images obtained by using different methods. Our proposed method achieves the highest PSNR and SSIM and lowest ARISM values among the competing methods, which indicates that our method can successfully enhance the overall quality of images and generate images that are visually more pleasant.

Fig. 6(a) is a test image chosen from the LOL dataset [7]. Fig. 6(i) is our result with $\lambda=0.01$ and $\mu=2$ by using the BM3D denoiser. From the comparison, we can clearly see that all methods can improve visual effect of such a low-light image to some extent. SR [20],

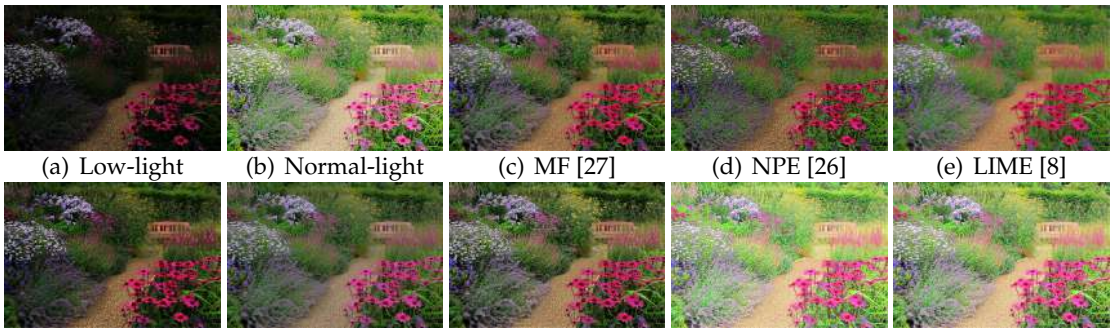

(a) Low-light (b) Normal-light (c) MF [27] (d) NPE [26] (e) LIME [8]

(f) LNet [34] (g) DCE [36] (h) LCR [25] (i) w/o denoiser (j) Ours

Figure 7: Enhancing results of state-of-the-art methods and ours on images from the NPE dataset [26]. (a) Low-light image, (b) normal-light image, (c)-(h) enhanced results by using other competing methods, (i) enhanced result by using our method without any denoiser, (j) enhanced result by using our method with RF denoiser.

Table 5: Quantitative analysis for Fig. 7.

	MF [27]	NPE [26]	LIME [8]	LNet [34]	DCE [36]	LCR [25]	w/o denoiser	**Ours**
PSNR	13.3928	12.9826	14.5336	10.4912	14.2942	13.6247	13.1376	**15.3001**
SSIM	0.6411	0.6428	0.6553	0.4266	0.7119	0.5912	0.7099	**0.7370**
ARISM	2.8449	2.8704	2.8439	2.8409	2.8363	2.8482	2.6179	**2.6129**

LCR [25] and LNet [34] can brighten the whole image slightly. LIME [8] over-enhances the input image that some low-illumination regions are saturated. EnGAN [35] can fully enhance the low-visibility regions, it also generates artifacts. MF [27] and DCE [36] fail to restore a low-light image, which result in unknown noises in the enhanced images. Additionally, in Table 4, we also see that our method gives the higher PSNR and SSIM and lower ARISM values compared with other competing methods. This means that our method presents satisfying performance handling low-light images both in visual terms and overall enhanced image evaluation.

Fig. 7 illustrates that our method can recover low-light images to match with human perception. Fig. 7(a) and (b) are low-light and normal-light images from the NPE dataset [26]. Fig. 7(i) and (j) are our enhanced results without any denoiser and with RF denoiser respectively by using $\lambda = 0.01$ and $\mu = 5$. As can be observed in visual comparisons, we can clearly see that all results generated by different methods can enhance the visibility of low-light images to some extent. However, our method can sufficiently light up the low-illumination image. From Fig. 7, we see that without any denoiser, the PSNR of our enhanced image is 13.1376 in Fig. 7(i). In contrast, the PSNR is boosted to 15.3001 by using the RF denoiser. It verifies the effectiveness of our method against other competing methods by using off-the-shelf denoisers in the second stage. In Table 5, we also report the PSNR, SSIM and ARISM values of enhanced images obtained by using different methods. In terms of three quantitative metrics mentioned above, our method is always best. It again indicates that our method can successfully improve visualization

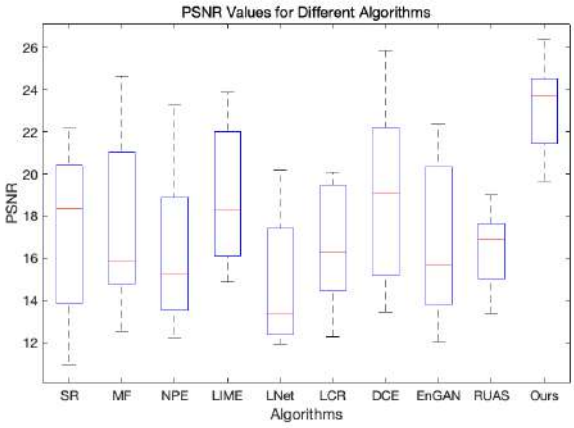

Figure 8: Box plot of the PSNR values for different algorithms.

and preserve the naturalness of the whole image.

In order to further demonstrate the generalization ability of our model, we evaluate the aforementioned methods on 30 low-light images collected from three challenging datasets: NPE dataset [26], LOL dataset [7], and GladNet dataset [56]. Fig. 8 describes box plot of PSNR values gained by our method and other state-of-the-art enhancement algorithms. As shown in Fig. 8. We find that the median of PSNR value gained by our method is significantly higher. Moreover, in Fig. 8, the top rectangular box indicates that our proposed method is more closer to a normal-light image with noise removal than other competing techniques. The failure cases exist in other competing enhancement algorithms mainly due to the unknown noise hidden in the dark areas, leading to unsatisfactory enhanced results.

5 Conclusion

In this paper, we propose a two-stage method for enhancing low-light images based on fractional-order differential. In the first stage, our method finds a piecewise smooth illumination map by solving a variational model with two regularization terms based on fractional differential. One regularization term serves the purpose of preserving structure similarity between the fractional derivative of the refined illumination and the fractional derivative of input images. The other regularization term is designed to constrain spatial smoothness on the estimated illumination. In the second stage, it uses a general image restoration model to recover a low-light image. It is worth noticing that the regularization term in the restoration part can be viewed as an adaptive mapping. Hence, various networks can be incorporated into our model and do not need to design any priors. Since the regularization term can be arbitrary, we can use different off-the-shelf denoisers to regularize the reflectance component and require no training at all. Comparisons with

state-of-the-art methods show that our proposed method can somehow enhance low-visibility images with satisfactory visual effects.

Acknowledgments

This work was supported in part by the National Key R&D Program of China under Grant 2021YFE0203700, Grant NSFC/RGC N_CUHK 415/19, Grant ITF MHP/038/20, Grant CRF 8730063, Grant RGC 14300219, 14302920, 14301121, and CUHK Direct Grant for Research under Grant 4053405, 4053460, in part by the National Natural Science Foundation of China under Grant 61902192, and in part by the High-Level Innovative and entrepreneurial project in Jiangsu Province, China (Jiangsu Personnel Office Document, No. [2019]20).

References

[1] Q. Ma, Y. Wang and T. Zeng, Low-light image enhancement via implicit priors regularized illumination optimization, IEEE Transactions on Computational Imaging, 9(2023), 944-953.
[2] M. Fan, W. Wang, W. Yang, J. Liu, Integrating semantic segmentation and retinex model for low-light image enhancement, in Proceedings of the 28th ACM International Conference on Multimedia, (2020), 2317-2325.
[3] L. Zhang, A. Zhu, Y. Shen, S. Zhao, H. Zhang, Revisit retinex theory: Towards a lightness-aware restorer for underexposed images, Mathematical Problems in Engineering, (2020), 1325705.
[4] X. Lv, Y. Sun, J. Zhang, F. Jiang, S. Zhang, Low-light image enhancement via deep retinex decomposition and bilateral learning, Signal Processing: Image Communication, 99 (2021), 116466.
[5] S. Hao, X. Han, Y. Guo, X. Xu, M. Wang, Low-light image enhancement with semi-decoupled decomposition, IEEE Transactions on Multimedia, 22 (12) (2020), 3025–3038.
[6] H. Lee, K. Sohn, D. Min, Unsupervised low-light image enhancement using bright channel prior, IEEE Signal Processing Letters, 27 (2020), 251–255.
[7] C. Wei, W. Wang, W. Yang, J. Liu, Deep retinex decomposition for low-light enhancement, British Machine Vision Conference, (2018).
[8] X. Guo, Y. Li, H. Ling, LIME: Low-light image enhancement via illumination map estimation, IEEE Transactions on Image Processing, 26 (2) (2016), 982–993.
[9] J. Dong, J. Pan, J. Ren, L. Lin, J. Tang, M. Yang, Learning spatially variant linear representation models for joint filtering, IEEE Transactions on Pattern Analysis and Machine Intelligence, (01) (2021), 1–1.
[10] W. Yang, W. Wang, H. Huang, S. Wang, J. Liu, Sparse gradient regularized deep retinex network for robust low-light image enhancement, IEEE Transactions on Image Processing 30 (2021) 2072–2086.
[11] Q. Dai, Y. Pu, Z. Rahman, M. Aamir, Fractional-order fusion model for low-light image enhancement, Symmetry, 11 (4) (2019), 574.
[12] M. Cheng, T. Huang, X. Zhao, T. Ma, J. Huang, A variational model with hybrid hyper-Laplacian priors for retinex, Applied Mathematical Modelling, 66 (2019), 305–321.

[13] S. Lim, W. Kim, DSLR: Deep stacked Laplacian restorer for low-light image enhancement, IEEE Transactions on Multimedia, 23 (2021), 4272–4284.
[14] X. Zhao, W. Xu, T. Jiang, Y. Wang, M. Ng, Deep plug-and-play prior for low-rank tensor completion, Neurocomputing, 400 (2020), 137–149.
[15] G. Hou, H. Pan, B. Huang, G. Wang, W. Wei, Z. Pan, Efficient L1-based nonlocal total variational model of retinex for image restoration, Journal of Electronic Imaging, 27 (5), (2018) 051207.
[16] M. Tang, F. Xie, R. Zhang, Z. Jiang, A. Bovik, A local flatness based variational approach to retinex, IEEE Transactions on Image Processing, 29 (2020), 7217–7232.
[17] R. Kimmel, M. Elad, D. Shaked, R. Keshet, I. Sobel, A variational framework for retinex, International Journal of Computer Vision, 52 (1) (2003), 7–23.
[18] I. Prior, Single image de-haze under non-uniform illumination using bright channel prior, Journal of Theoretical and Applied Information Technology, 48(3) (2013), 1843–1848.
[19] Y. Wang, S. Zhuo, D. Tao, J. Bu, N. Li, Automatic local exposure correction using bright channel prior for under-exposed images, Signal processing, 93 (11) (2013), 3227–3238.
[20] M. Li, J. Liu, W. Yang, X. Sun, Z. Guo, Structure-revealing low-light image enhancement via robust retinex model, IEEE Transactions on Image Processing, 27 (6) (2018), 2828–2841.
[21] Z. Gu, F. Li, F. Fang, G. Zhang, A novel retinex-based fractional-order variational model for images with severely low light, IEEE Transactions on Image Processing, 29 (2019), 3239–3253.
[22] S. Park, S. Yu, B. Moon, S. Ko, J. Paik, Low-light image enhancement using variational optimization-based retinex model, IEEE Transactions on Consumer Electronics, 63 (2) (2017), 178–184.
[23] X. Fu, D. Zeng, Y. Huang, X. Ding, X. Zhang, A variational framework for single low light image enhancement using bright channel prior, IEEE Global Conference on Signal and Information Processing, (2013), 1085–1088.
[24] Z. Gu, F. Li, X. Lv, A detail preserving variational model for image retinex, Applied Mathematical Modelling, 68 (2019), 643–661.
[25] Y. Ren, Z. Ying, T. H. Li, G. Li, LECARM: Low-light image enhancement using the camera response model, IEEE Transactions on Circuits and Systems for Video Technology, 29 (4) (2018), 968–981.
[26] S. Wang, J. Zheng, H. Hu, B. Li, Naturalness preserved enhancement algorithm for non-uniform illumination images, IEEE Transactions on Image Processing, 22 (9) (2013), 3538–3548.
[27] X. Fu, D. Zeng, Y. Huang, Y. Liao, X. Ding, J. Paisley, A fusion-based enhancing method for weakly illuminated images, Signal Processing, 129 (2016), 82–96.
[28] T. Wu, W. Li, S. Jia, Y. Dong, T. Zeng, Deep multi-level wavelet-cnn denoiser prior for restoring blurred image with cauchy noise, IEEE Signal Processing Letters, 27 (2020), 1635–1639.
[29] F. Fang, J. Li, Y. Yuan, T. Zeng, G. Zhang, Multilevel edge features guided network for image denoising, IEEE Transactions on Neural Networks and Learning Systems, 32 (9) (2021), 3956–3970.
[30] L. Ma, R. Liu, J. Zhang, X. Fan, Z. Luo, Learning deep context-sensitive decomposition for low-light image enhancement, IEEE Transactions on Neural Networks and Learning Systems, 33(10)(2022), 5666-5680.
[31] Q. Jiang, Y. Zhang, F. Bao, X. Zhao, C. Zhang, P. Liu, Two-step domain adaptation for underwater image enhancement, Pattern Recognition, 122 (2022), 108324.
[32] J. Li, J. Li, F. Fang, F. Li, G. Zhang, Luminance-aware pyramid network for low-light image

enhancement, IEEE Transactions on Multimedia, 23 (2021), 3153–3165.
[33] R. Liu, L. Ma, J. Zhang, X. Fan, Z. Luo, Retinex-inspired unrolling with cooperative prior architecture search for low-light image enhancement, in Proceedings of the IEEE/CVF Conference on Computer Vision and Pattern Recognition, (2021), 10561–10570.
[34] C. Li, J. Guo, F. Porikli, Y. Pang, LightenNet: A convolutional neural network for weakly illuminated image enhancement, Pattern Recognition Letters, 104 (2018), 15–22.
[35] Y. Jiang, X. Gong, D. Liu, Y. Cheng, C. Fang, X. Shen, J. Yang, P. Zhou, Z. Wang, EnlightenGAN: Deep light enhancement without paired supervision, IEEE Transactions on Image Processing, 30 (2021), 2340–2349.
[36] C. Guo, C. Li, J. Guo, C. C. Loy, J. Hou, S. Kwong, R. Cong, Zero-reference deep curve estimation for low- light image enhancement, in Proceedings of the IEEE/CVF Conference on Computer Vision and Pattern Recognition, (2020), 1780–1789.
[37] L. Wang, Z. Liu, W. Siu, D. Lun, Lightening network for low-light image enhancement, IEEE Transactions on Image Processing, 29 (2020), 7984–7996.
[38] W. He, Y. Liu, J. Feng, W. Zhang, G. Gu, Q. Chen, Low-light image enhancement combined with attention map and u-net network, in 2020 IEEE 3rd International Conference on Information Systems and Computer Aided Education, (2020), 397–401.
[39] S. Malik, R. Soundararajan, Llrnet: A multiscale subband learning approach for low light image restoration, in 2019 IEEE International Conference on Image Processing, (2019), 779–783.
[40] K. Xu, X. Yang, B. Yin, R. W. Lau, Learning to restore low-light images via decomposition and enhancement, in Proceedings of the IEEE/CVF Conference on Computer Vision and Pattern Recognition, (2020), 2281–2290.
[41] X. Song, J. Huang, J. Cao, D. Song, Multi-scale joint network based on retinex theory for low-light enhancement, Signal, Image and Video Processing, (2021), 1–8.
[42] F. Dong, Q. Ma, Single image blind deblurring based on the fractional-order differential, Computers & Mathematics with Applications, 78 (6) (2019), 1960–1977.
[43] Q. Ma, Y. Wang, and T. Zeng, Retinex-based variational framework for low-light image enhancement and denoising, IEEE Transactions on Multimedia, 25(2023), 5580-5588.
[44] Q. Ma, F. Dong, D. Kong, A fractional differential fidelity-based PDE model for image denoising, Machine Vision and Applications, 28 (5) (2017), 635–647.
[45] H. Lee, K. Sohn, D. Min, Unsupervised low-light image enhancement using bright channel prior, IEEE Signal Processing Letters, 27 (2020), 251–255.
[46] F. Dong, Y. Chen, A fractional-order derivative based variational framework for image denoising, Inverse Problems and Imaging, 10 (1) (2016), 27.
[47] Y. Zhang, N. Zhang, D. Sun, K. Toh, A proximal point dual Newton algorithm for solving group graphical Lasso problems, SIAM Journal on Optimization, 30 (3) (2020), 2197–2220.
[48] P. Tang, C. Wang, D. Sun, K. Toh, A sparse semismooth Newton based proximal majorization- minimization algorithm for nonconvex square-root-loss regression problems, Journal of Machine Learning Research, 21 (226) (2020), 1–38.
[49] S. Boyd, N. Parikh, E. Chu, B. Peleato, J. Eckstein, Distributed optimization and statistical learning via the alternating direction method of multipliers, Now Foundations and Trends, 2011.
[50] C. Chen, G. Xu, A new linearized split Bregman iterative algorithm for image reconstruction in sparse-view X-ray computed tomography, Computers and Mathematics with Applications, 71(8) (2016), 1537-1559.
[51] Y. Wang, W. Yin, J. Zeng, Global convergence of ADMM in nonconvex nonsmooth optimization, Journal of Scientific Computing, 78 (1) (2019), 29–63.

[52] T. Goldstein, S. Osher, The split Bregman method for L1-regularized problems, SIAM Journal on Imaging Sciences, 2 (2) (2009), 323–343.
[53] D. Geman, C. Yang, Nonlinear image recovery with half-quadratic regularization, IEEE Transactions on Image Processing, 4 (7) (1995), 932–946.
[54] K. Dabov, A. Foi, V. Katkovnik, K. Egiazarian, Image denoising by sparse 3-D transform-domain collaborative filtering, IEEE Transactions on Image Processing, 16 (8) (2007), 2080–2095.
[55] E. Gastal, M. Oliveira, Domain transform for edge-aware image and video processing, ACM Siggraph, (2011), 1–12.
[56] W. Wang, C. Wei, W. Yang, J. Liu, GLADNet: Low-light enhancement network with global awareness, In 2018 IEEE International Conference on Automatic Face and Gesture Recognition, (2018), 751–755.
[57] A. Hore, D. Ziou, Image quality metrics: PSNR vs. SSIM, 20th International Conference on Pattern Recognition, (2010), 2366–2369.
[58] Z. Wang, A. C. Bovik, H. R. Sheikh, E. P. Simoncelli, Image quality assessment: Rrom error visibility to structural similarity, IEEE Transactions on Image Processing, 13 (4) (2004), 600–612.